

# A TWO-TYPE CLASSIFICATION OF LASCO CORONAL MASS EJECTION

M. D. ANDREWS<sup>1</sup> and R. A. HOWARD<sup>2</sup>

<sup>1</sup>*Computational Physics, Inc., Fairfax, VA, U.S.A. (e-mail: andrews@louis14.nrl.navy.mil)*

<sup>2</sup>*E.O. Hulburt Center for Space Research, Naval Research Laboratory, Code 7660, Washington DC 20375, U.S.A.*

**Abstract.** The causes and origins of Coronal Mass Ejections (CMEs) remain among the outstanding questions in Space Physics. The observations of CMEs by the LASCO coronagraphs on SOHO suggest that there are two distinct types of CMEs. The two types of events can be most easily distinguished by examining height-time plots. The Type A (Acceleration) events produce curved plots that often indicate a constant acceleration. These events are usually associated with pre-existing helmet-streamers, and are often associated with prominence eruptions or filament disappearance. The Type C (Constant speed) events show a constant speed. These events are usually brighter, larger, and faster than Type A events and may be associated with X-ray flares. While the two types of events can be distinguished in other ways, the height-time plots are a simple and unambiguous way to make this identification.

## 1. Introduction

The cause(s) and origin(s) of Coronal Mass Ejections (CMEs) is one of the key, long-standing, and unresolved issues of Space Physics. CMEs were first identified as a geophysical phenomenon only after data from the first space-borne coronagraphs were analyzed (Tousey, 1973). Two excellent reviews of CMEs appeared in *Coronal Mass Ejections* (Crooker *et al.*, 1997). Gosling (1997) summarizes the understanding of CMEs and lists the following questions: “What is the physics of initiation and what are its signatures? What determines when and where a CME will occur and how fast the ejection of material will be? What are the processes by which CMEs are accelerated?” Hundhausen (1997, and references therein) summarized the observation basis of the empirical knowledge of CMEs. He states, “It is clear that many puzzles remain concerning the physical causes of coronal mass ejections and that those puzzles raise serious difficulties in any attempt to predict earth-directed mass ejections and their interplanetary and geomagnetic consequences.”



In this review, we will present observations from the LASCO<sup>1</sup> coronagraphs to support the suggestion that there are two distinct types of CMEs. The two types of CMEs are most easily distinguished by examining plots of height versus time (H-T plots). The first class of CMEs, Type A, have H-T plots that show acceleration. The second class of events, Type C, have H-T plots with constant speed. The distinction is between events with acceleration, Type A, and events with constant speed, Type C. This review will be presented from an observational perspective only. Wu, Andrews, and Plunkett (2000) consider the analysis and modeling of CMEs.

This distinction is not new. MacQueen and Fischer (1983) analyzed 12 well-observed coronal transients. They conclude that these events represented two classes that could be clearly delineated based on plots of radial speed versus height. They identify the two classes as (1) flare-associated, impulsive events with a constant speed, and (2) eruptive-associated events that show significant acceleration. They offer the suggestion that flare-associated transients and eruptive associated events may be fundamentally different.

A number of excellent reviews of CME observations have been published (Wagner, 1984; Howard *et al.*, 1985; Kahler, 1987; Hundhausen, 1993; Low, 1996, among others). Attempts have been made to understand the origins of CMEs by examining the correlation between mass ejections and other types of solar activity. Gosling *et al.* (1976) demonstrated that CMEs were associated with either flares or eruptive prominences. The flare-associated CMEs were found to be faster, were more likely to be associated with Type II and Type IV radio bursts, and were more likely to produce significant shocks at 1 AU. Munro *et al.* (1979) examined 115 coronal transients observed by the High Altitude Observatory (HAO) coronagraph on *Skylab* (1973–1974). They conclude that 40% of the ejections could be associated with flares and that 50% were associated with eruptive prominences or disappearing filaments without flares. Webb and Hundhausen (1987) studied CMEs observed by the Solar Maximum Mission (SMM, 1980 and 1984–1989) coronagraph. They found that the majority of CMEs were associated with eruptive prominences. They also reported that the majority of SMM CMEs showed significant acceleration. These accelerated CMEs were slower and usually associated with eruptive prominences.

Kahler (1992) reviewed our understanding of the relationship between flares and CMEs. He states that the relationship between flares and CMEs is unclear and concludes that flares appear to be a *consequence* (emphasis added) of CMEs. Dryer

<sup>1</sup>LASCO is the Large Angle Spectroscopic Coronagraph which is one of the instruments on the Solar and Heliospheric Observatory (SOHO) which is a mission of international cooperation between NASA and ESA. The LASCO experiment was developed by a consortium of institutions from four countries: E. O. Hulburt Center for Space Research, Naval Research Laboratory, Washington, DC; Laboratoire d'Astronomie Spatiale, Marseille, France; Max-Planck-Institut für Aeronomie, Lindau, Germany; and Space Research Group, School of Physics and Space Research, University of Birmingham, Birmingham, U.K.

(1996) reviews the existing observations and modeling to conclude: “CMEs can be generated either by flares or by large-scale helmet disruptions. I therefore suggest that these works support the concept of a bimodal set of causes for the origin of CMEs.”

St. Cyr *et al.* (1999) have reported an analysis of 246 CMEs observed by the MK3 coronagraphs at the Mauna Loa Solar Observatory from 1980 through 1989. For 140 of these events, the data quality was sufficient to measure the apparent speed. In only 13 of 140 (9%) was a significant acceleration measured. They considered 55 CMEs observed by both MK3 and SMM. For these events, there were 76 features for which a combined MK3-SMM height-time analysis could be done. A constant speed was determined in only 36 cases with the other 40 features being fit by a constant acceleration. They indicate that, for the accelerated features, the launch height of the CME was significantly above the photosphere. This study clearly demonstrated that the quantitative measurement of CME properties is strongly dependent on the heights over which the event is measured.

## 2. LASCO Observations

In the paragraphs above, we have briefly summarized the understanding of CMEs that existed prior to the launch of the SOHO spacecraft in December 1995 (Fleck *et al.*, 1995). The LASCO instruments (Brueckner *et al.*, 1995) have yielded greatly improved observations of CMEs. Howard *et al.* (1997) presented the initial results from LASCO.

The LASCO instruments represent a significant improvement over previous satellite coronagraphs due to several complimentary factors. The telescopes have a significantly reduced stray-light level. The detectors are cooled CCDs that have a very low noise-level and a large dynamic-range. Another important factor is the L-1 orbit of SOHO. This location results in a much more stable viewing geometry that is particularly important for the observations of CMEs. CMEs are seen as a transient brightening of the corona. While CMEs can occasionally be seen in raw images from LASCO C2, the viewing of CMEs typically requires the subtraction of a pre-event or background image. The remarkable stability of the LASCO instruments yields very much improved difference images.

In this paper, we present observations from the C2 and C3 coronagraphs on LASCO. Both instruments are externally occulted, Lyot (1930) coronagraphs. The C3 telescope design is similar to that of the NRL developed coronagraphs on OSO-7 (Koomen *et al.*, 1975) and SOLWIND. The C2 telescope is similar with an improved occulter. Both instruments have  $1024 \times 1024$  CCD cameras in the focal plane. The C2 telescope images the region from approximately 2.0 to 6.0  $R_{\odot}$  with a resolution of  $\sim 23''$  and a pixel size of  $11.9''$ . The C3 telescope images the region of approximately 3.7 to 32  $R_{\odot}$  with a resolution of  $\sim 113''$  and a pixel size of  $56''$ .

The LASCO observations yield significantly improved H–T plots. CMEs are seen much more clearly so that individual features are more easily identified and tracked. The combination of data from the C2 and C3 instruments allows the routine tracking of CMEs from initial heights of less than  $3 R_{\odot}$  to  $20\text{--}30 R_{\odot}$ . The resulting H–T plots have more data points due to the greater height range with the individual points being more accurately measured. In the following sections, we present two examples of each type of CME. The events presented herein are not typical. They were selected to illustrate the key features of each type of event. CMEs often have complex structures that may change significantly as the CME develops and moves away from the Sun. This dynamic evolution cannot be fully illustrated by still images. The dynamics of CMEs can be much more easily seen in data animations (movies) generated from the LASCO data. Two movies have been produced for each of the example CMEs, one each for the C2 and C3 images of the event. These movies are available on the web in mpeg format (<ftp://ares.nrl.navy.mil/pub/lasco/andrews/>).

### 3. Type A Events

The Type A events show significant acceleration in the C2 and/or C3 Fields-of-View (FOV). These events tend to have complex structures that show significant changes as they propagate away from the Sun, are associated with the disruption and ejection of helmet-streamers, and often coincide with prominence eruptions and/or filament disappearance.

The first example event, CME1, was observed above the west limb of the Sun on June 22, 1998. Four images of this CME are shown in Figure 1. (See Wu *et al.*, 1997, for information on how the LASCO images were processed.) Figure 1(a) shows the pre-event corona a few hours before the CME. A helmet-streamer is seen approximately  $40^{\circ}$  north of the equator. This streamer brightens and thickens for several hours before the CME is first visible as a distinct structure early on June 22, 1998. Accelerated CMEs often show complex structures that change significantly as the CME develops and moves away from the Sun. This dynamic evolution cannot be fully illustrated by the four images in Figure 1. The reader is strongly encouraged to examine the above referenced movies.

Figure 1(b) shows CME1 as it nears the edge of the C2 FOV. CME1 now exhibits the classic three-part structure of a CME as defined by Kahler (1988): a bright leading edge surrounding a dark cavity that contains a bright knot. Figure 1(c) shows CME1 near the middle of the C3 FOV. The structure of CME1 has changed significantly. The leading edge of CME1 now shows two loop-like structures and the shape of the bright knot is much different.

Four features, A, B, C, and D in Figure 1(c), were tracked through the C2 and C3 images to generate the H–T plot shown in Figure 2(a). The four features are the leading edges of two loops (A and B) and the front and back of the bright knot (C

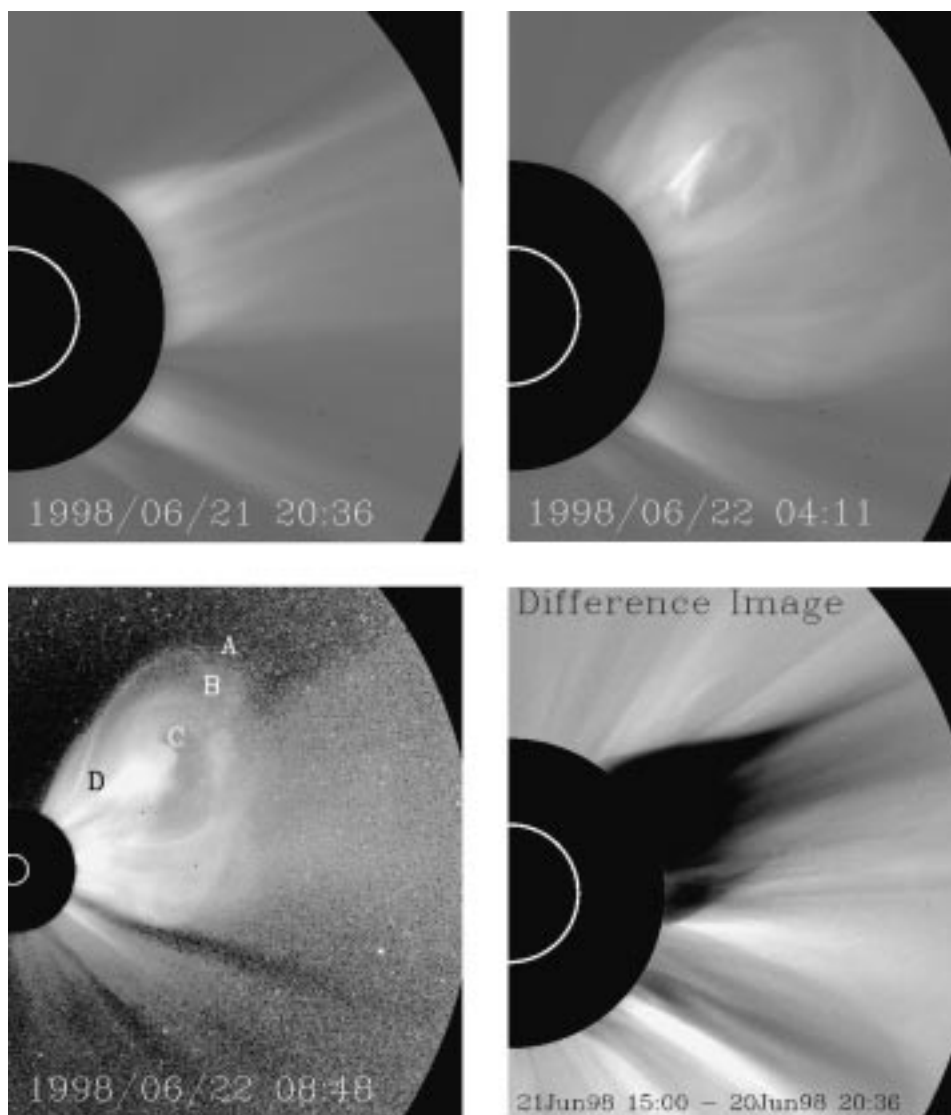


*Figure 1.* Four LASCO partial frame images of a Type A CME observed June 22, 1998. (a) shows a C2 image of the west limb of the Sun prior to the CME. A large helmet-streamer is seen to the north of the equator. (b) shows the CME near the center of the C2 FOV as a large loop containing a bright core. (c) shows the CME near the middle of the C3 FOV. Two loops are seen surrounding the bright core. The features A, B, C, and D identify the two loops and the front and back of the bright knot. (d) is a C2 difference image showing the disappearance of the helmet streamer. In each of the LASCO images, the bright ring indicates the location of the solar limb.

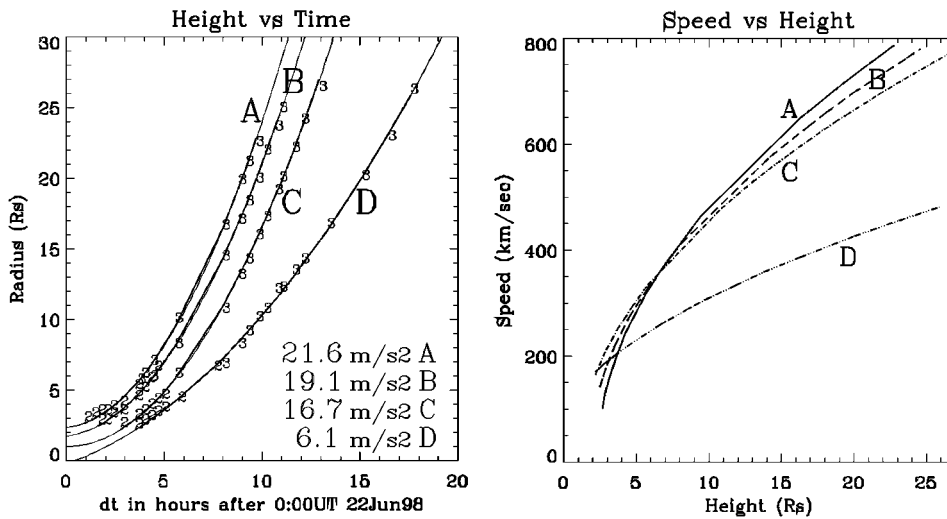


Figure 2. H-T plot of the four features identified in Figure 1(c). (a) displays the measured height versus time for CME1. The C2 (C3) positions are indicated by 2 (3). The uncertainty in the position is approximately the size of the symbol. Also shown is a second order fit, constant acceleration, to the data points and the acceleration obtained from the fit. (b) shows speed versus height derived from the curves of (a).

and D). The C2 and C3 data points are shown along with the constant acceleration fit to the data. Figure 2(b) shows the speed versus height for CME1 based on the constant acceleration fit to the data as shown in Figure 2(a). This event shows accelerations and speeds that are unusually high for Type A CMEs. Features A, B, and C all have speeds that approach 800 km/sec at heights above 20  $R_{\odot}$ . The speed of feature D is smaller but is still significantly faster than is common for events of this type. These speeds are higher than is observed in the slow solar wind.

Figure 1(d) is a C2 difference image of the corona before and after CME1. The helmet-streamer is gone and the area of the pre-event streamer is significantly less bright than the surrounding areas. CME1 had little effect on the other coronal structures. The changes in the southwest are primarily due to rotation.

Unpublished LASCO data collected using a narrow-band  $H\alpha$  filter show that CME1 contains prominence material. C2 images of the bright core show  $H\alpha$  emission at heights of less than 6  $R_{\odot}$ . (There is no significant  $H\alpha$  emission detected in the C3 images.)  $H\alpha$  images from the Observatoire De Paris Spectroheliograph show a dark filament on June 20 and 21 that is clearly missing from the image of 22 June, 1998. The prominence eruption occurred above the west limb at the location of the helmet streamer. All of the observations indicate that CME1 is nearly in the plane of the sky. Projection effects are unimportant for this event and the measured accelerations and speeds are close to the actual radial values.

The second example event, CME2, was observed on August 13–14, 1997 (Andrews and Howard, 1999). This particular CME was observed simultaneously by

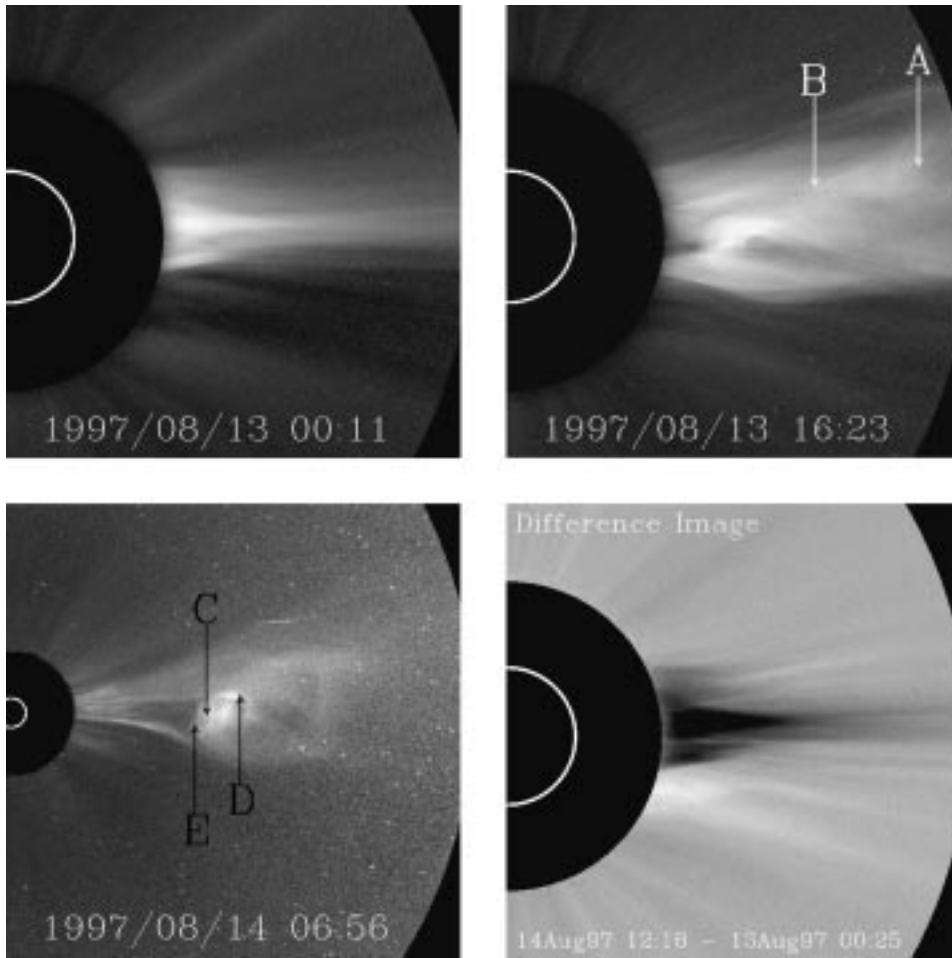


Figure 3. Four LASCO partial frame images of a Type A CME observed August 14, 1997. (a) shows a C2 image of the west limb of the Sun prior to the CME. A single helmet-streamer is seen on the equator. (b) shows the CME in the C2 FOV. The CME is seen as a complex set of bright structures. The leading edge of the CME has separated to form a V-shaped structure. The features A and B are the front and rear of this structure. (c) shows the CME near the middle of the C3 FOV. The structure is seen as a large, faint loop containing a bright, complex core. The features C, D, and E are the rear of the bright knot, the front of the bright knot, and the rear edge of the loop. (d) is the difference of C2 images showing the disappearance of the helmet-streamer. In each of the LASCO images, the bright ring indicates the location of the solar limb.

the UVCS instrument on SOHO (Strachan *et al.*, 1999). The pre-event coronal structures are very simple as shown in Figure 3(a). There is a single streamer located above the solar equator. This streamer brightens and widens over a period of two days prior the eruption. CME2 is a very dynamic event. There are a number of complex structures that change dramatically as the event evolves and moves

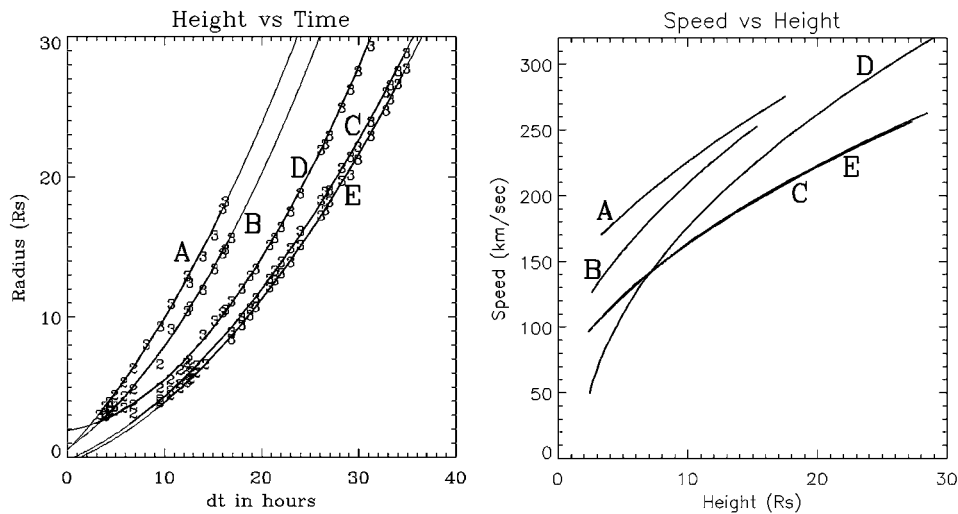


Figure 4. H-T plot of the five features identified in Figures 3(b) and (c). (a) displays the measured height versus time for CME2. The C2 (C3) positions are indicated by 2 (3). The uncertainty in the position is approximately the size of the symbol. Also shown is a second order fit, constant acceleration, to the data points. (b) shows speed versus height derived from the curves of (a).

away from the Sun. (The dynamics of this CME can not be adequately represented in Figure 3; the reader is directed to the above referenced movies.)

Figure 3(b) shows CME2 near the edge of the C2 FOV. The leading, upper portion of CME2 has separated from the rest of the event and shows a distinct V-shaped structure. Features A and B are the front and rear of this structure. Figure 3(c) shows CME2 in the middle of the C3 FOV. Features A and B have faded from view. A bright, complex knot is seen near the rear of CME2. The features C, D, and E are the rear of the bright knot, the front of the bright knot, and the rear edge of the trailing loop. This loop remains visible throughout the C3 FOV.

Figure 3(d) shows the C2 difference image of the corona before and after CME2. The pre-event helmet-streamer has disappeared. The high-latitude corona remains unchanged. The equatorial streamer has been completely removed and this region is significantly less bright than the nearby, quiet corona.

Figure 4(a) presents the H-T plot for the five features of CME2. All of the data are well fit by the second-order, constant acceleration curves. Figure 4(b) shows the plot of speed versus height derived from the constant acceleration fit to the data. Features A and B are faint and fade from view at low heights. Both of these observations suggest that these features are located well out of the sky plane. The angle of these two structures from the sky plane is not known. However, it is likely that projection effects are important. Features A and B show larger projected accelerations and speeds than the other three features tracked. Furthermore, it is likely that the measured values for features A and B are significantly less than the radial values.

For features C, D, and E the observations indicate that these structures are at small angles from the sky plane. Unpublished analysis of LASCO polarization sequences of the bright core indicates that this structure is within  $20^\circ$  of the sky plane. The UVCS observations (Strachan *et al.*, 1999) show no significant Doppler shift in the observed lines. While the observed accelerations and speed for features B, C, and D are very small, it is likely that they are close to the radial values.

The bright knot at the rear of CME2 is probably prominence material. The UVCS observations show the knot to consist of cool, dense material (Strachan *et al.*, 1999). The LASCO data indicate a peak density of greater than  $1 \times 10^{+5} \text{ e}^-$  or  $\text{cm}^{-3}$  (Andrews and Howard, 1999).

In the above paragraphs, we have briefly summarized the observations of two Type A CMEs. The two events cannot be considered typical. CME1 is larger and much faster than is typical. CME2 is smaller, slower, and has more complicated structures than is typical. These two events represent extreme examples. However, they do illustrate the key observational characteristics of the Type A events. The H-T plots of individual features are very well fit by a constant acceleration throughout the C2 and C3 FOVs. Both events consist of the eruption and removal of a pre-existing helmet-streamer. For both events, the leading edge of the CME originates at heights of  $2-3 R_\odot$ . These events show complex, changing structures that include a bright loop with a dark interior and a bright knot within the loop that observations indicate is prominence material.

#### 4. Type C Events

Type C events show constant speed in the C3 FOV, and usually show constant speed when C2 data is combined with C3. While these events often do have complex structure, the structures do not usually change as the CMEs move away from the Sun. Some Type C events are observed to be temporally coincident with large X-ray flares.

The first example event, CME3, was observed on November 6, 1997. This CME was coincident with the brightest X-ray flare observed since the launch of SOHO. The flare began at 11:49 UT on November 6, 1997 and reached a peak brightness of  $9.4 \times 10^{-4} \text{ W m}^{-2}$ , X9.4, at 12:01 UT. The flare was located at  $18^\circ$  S latitude,  $63^\circ$  W longitude and was associated with NOAA active region 8100. This active region was the source of a halo CME, possibly flare associated, on November 4, 1997 which produced a significant geo-magnetic storm at Earth. This period has been selected as an ISTP Sun–Earth Connection Event (<http://www-spf.gsfc.nasa.gov/istp/events>).

The LASCO observations of CME3 are presented in Figure 5. Figure 5(a) is a C2 image of the west limb of the Sun. The observed structures are the result of a series of energetic CMEs observed on the previous days and are not typical of the quiet corona (compare with Figure 3(a)). Figure 5(b) is a C2 image recorded

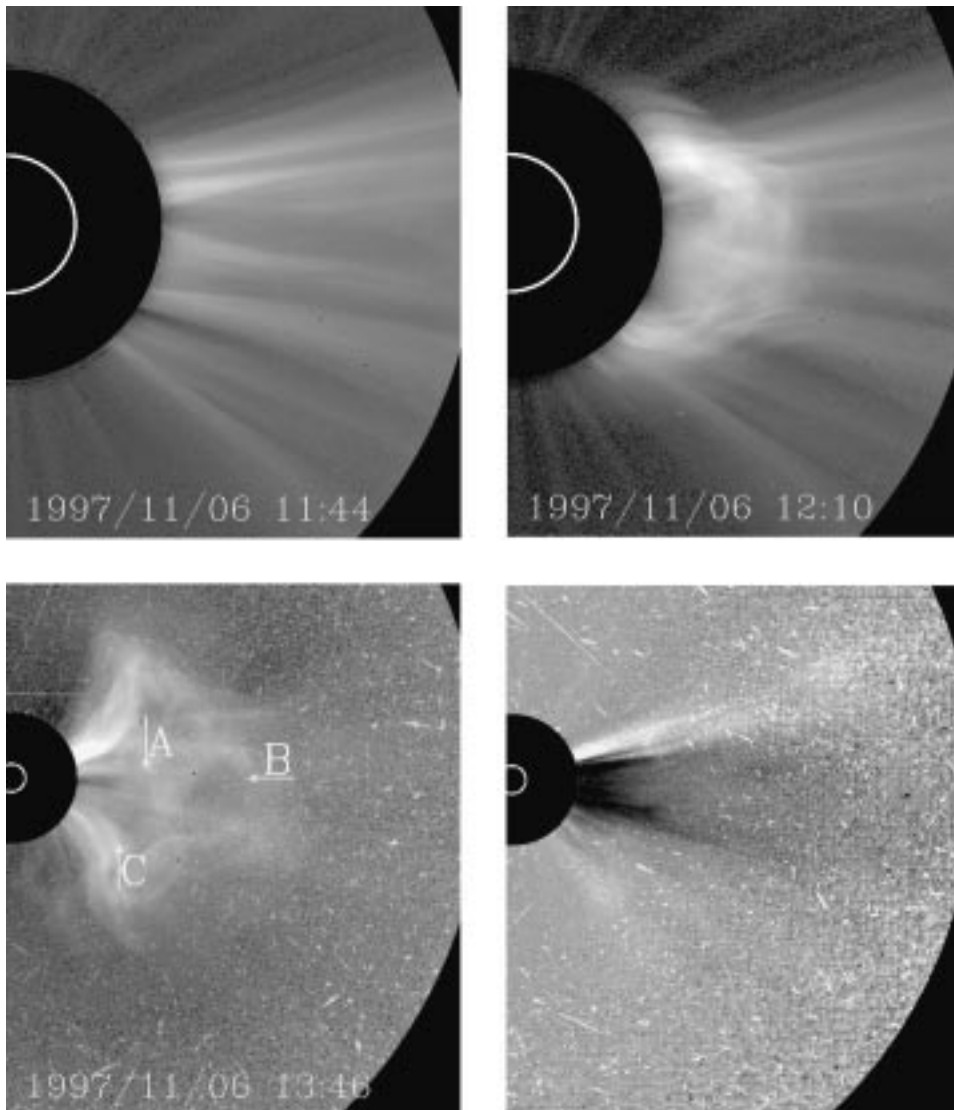


*Figure 5.* Four LASCO partial frame images of a Type C CME observed November 6, 1997. (a) shows a C2 image of the west limb of the Sun prior to the CME. The observed radial structures are the consequence of a series of CMEs on the previous days. (b) is the first image of CME3 recorded 26 min after the previous image. CME3 is seen as a series of bright arcs extending over about  $90^\circ$  in latitude. (c) shows CME3 near the middle of the C3 FOV. The shape of CME3 has changed due to the dramatic extension of the flanks of the CME. The feature B is a bright arc slightly behind the leading edge; features A and C are bright knots that were identified in several images. (d) is a C3 difference image. The corona above the equator is significantly dimmer and the streamers to the north and south of the equator have been deflected to higher latitudes. The bright, cluttered background is due to a large Solar Energetic Particle event. In each of the LASCO images, the bright ring indicates the location of the solar limb.

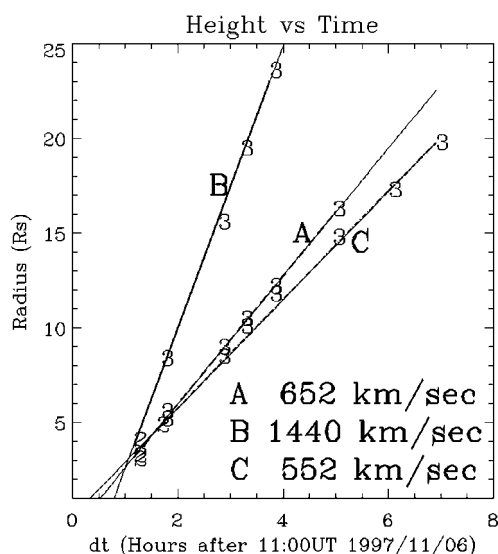


Figure 6. H-T plot of the three features identified in Figure 5(c). The C2 (C3) positions are indicated by 2 (3). The uncertainty in the position is approximately the size of the symbol. Also shown are the linear fits to the data and the speeds obtained from the fits.

26 min later. CME3 is large, bright, and has already propagated well into the C2 FOV. In Figure 5(b), the CME3 has the appearance of a number of bright arcs and knots that extend over about  $90^\circ$  in latitude. CME3 is shown near the middle of the C3 FOV in Figure 5(c). The CME looks very different due to the dramatic extension of the flanks of the event to the north and south. The structures closer to the equator have not changed significantly. This CME does not show the three-part structure seen in Figures 1 and 3.

Figure 5(d) shows the difference in the C3 corona before and after the CME. The corona above the equator is significantly dimmer than prior to the event. The streamers to the north and south of the equator have been deflected toward the poles by the CME. CME3 and/or the X-flare caused a large Solar Energetic Particle (SEP) event the effect of which is visible in Figure 5(d). The CCD detectors of LASCO 'see' the energetic particles to produce a bright, cluttered background. For CME3, the background became so intense that the CME was obscured before reaching the limits of the C3 images.

Figure 6 displays the H-T plot for the three features labeled A, B, and C in Figure 5(c). Feature B is a bright arc slightly behind the leading edge near the equator. Features A and C indicate bright knots that could be identified in several images. The measurements are well fit by constant speeds that range from 550 to  $1440 \text{ km s}^{-1}$ . The speed of feature B is much larger than for features A and C. It is unlikely to be due to projection effects and probably represents an actual velocity difference.

CME3 is not a typical event. It is one of the brightest and fastest CMEs observed by LASCO. Observations of this event from the Orporto radiospectrograph and the Nancay radioheliograph have been analyzed along with LASCO C1, C2 and C3 coronagraph data as reported by Maia *et al.* (1999). Strong radio emission is observed beginning about 11:52 UT on November 6, 1997. The radio source is initially observed to occupy a small area near the flare site but rapidly expands to cover about  $100^\circ$  in latitude. The X-ray flare, the radio emission, and the launch of the CME occur simultaneously within a timing accuracy of a few minutes.

The final example event, CME4, was observed on October 6, 1996. The observation and modeling of this event has been presented by Andrews *et al.* (1999). CME4 is modeled using a 2-dimensional, bimodal model for the pre-event corona and a time dependent perturbation at the base of the corona, e.g., a pressure pulse.

Figure 7(a) is a pre-event C2 image of the west limb of the Sun. The pre-event structures consist of streamers north and south of the equator visible to the limits of the C3 FOV plus a fainter structure near the equator. Figure 7(b) shows CME4 near the middle of C2 FOV. The CME is seen as a circular arc that extends from near the north-pole to the equator and extends to the southern edge of the southern streamer in the form of a more ragged arc. The pre-event structures remain clearly visible. Figure 7(c) shows CME4 in the middle of the C3 FOV. Figures 7(b) and 7(c) look very similar. The structures do not change significantly as the CME moves away from the Sun. CME4 also shows no sign of the three-part structure seen for CME1 and CME2.

Figure 7(d) displays the difference of a pre-event and post-event C2 images. During this time period, static coronal structures would have rotated through  $20^\circ$ . The alternating dark and bright lanes in Figure 5(d) are probably due to this rotation. The differences that are attributed to the CME are small. CME4 has produced little change in the corona.

Figure 8 is the H-T plot for the three features identified in Figure 7(c): the leading edge at a position north of the northern streamer, a point on the arc near the equator, and the southern edge of the bright arc. The lines in Figure 8 are a constant-speed fit based on the C3 data only, i.e., the C2 data points were not used in determining the fit. The speeds range from 620 to 360  $\text{km s}^{-1}$ . The fit to the C3 data is good especially at heights above about  $6 R_\odot$ . The fit to the C2 points is not as good. The C2 data points are all located to the left of the constant speed curves. This probably indicates some acceleration for these features at low heights. This acceleration is not large, and when the C2 and C3 data are combined to determine the constant speed each of the features is well fit by a straight line.

There was no observed solar activity associated with CME4. CME4 was assumed to be associated with a region of activity that was about  $30^\circ$  behind the west limb at the time of the CME. The modeling of this event explains the differences in the observed speeds as due to the state of the pre-event corona rather than projection effects.

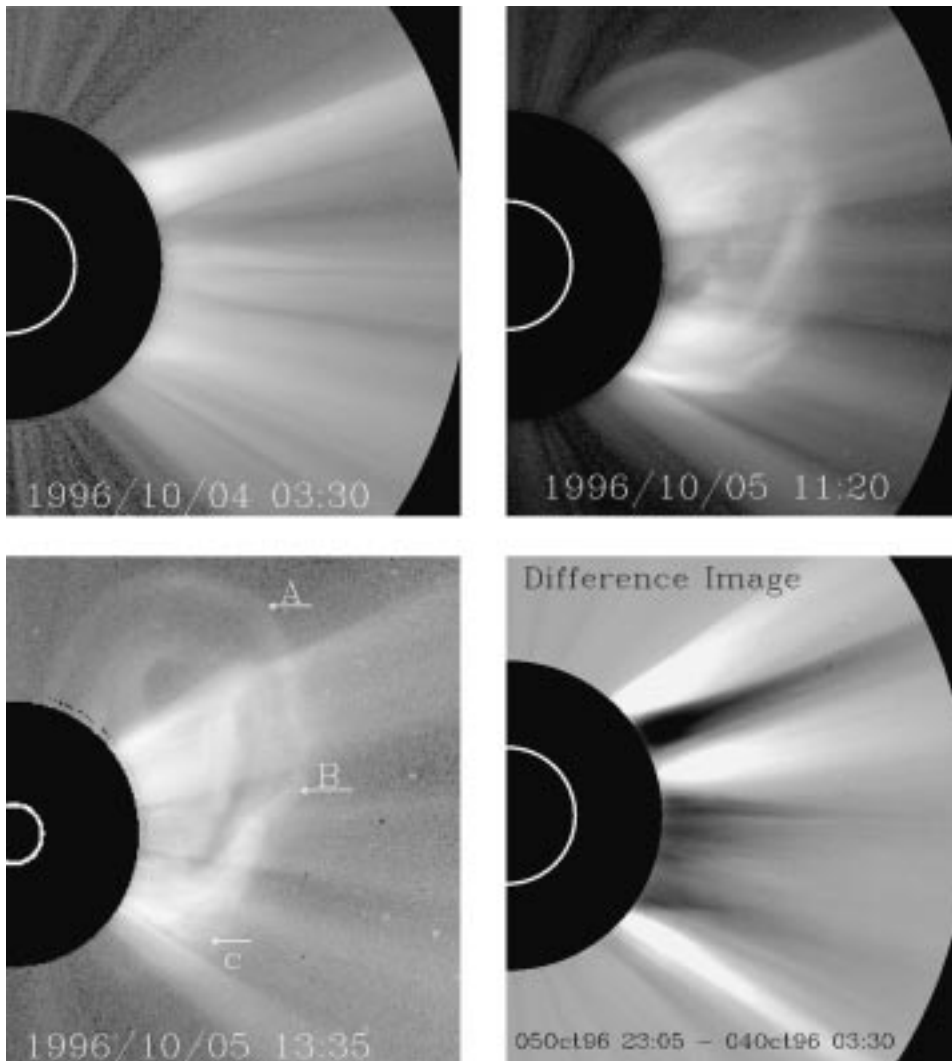


Figure 7. Four LASCO partial frame images of a Type C CME observed October 6, 1997. (a) shows a C2 image of the west limb of the Sun prior to the CME. Helmet-streamers are seen both above and below the equator with faint structures seen near the equator. (b) shows CME4 in the C2 FOV. CME4 is seen as bright circular arc extending from near the north pole to the equator with a less regular extension to the edge of the southern streamer. The structures seen in (a) remain visible. (c) shows CME4 near the middle of the C3 FOV. The structure of CME4 has not changed significantly. The labels A, B and, C indicate three positions on the leading edge of CME4. (d) is a C2 difference. The differences are primarily due to rotation rather than actual changes in the corona. In each of the LASCO images, the bright ring indicates the location of the solar limb.

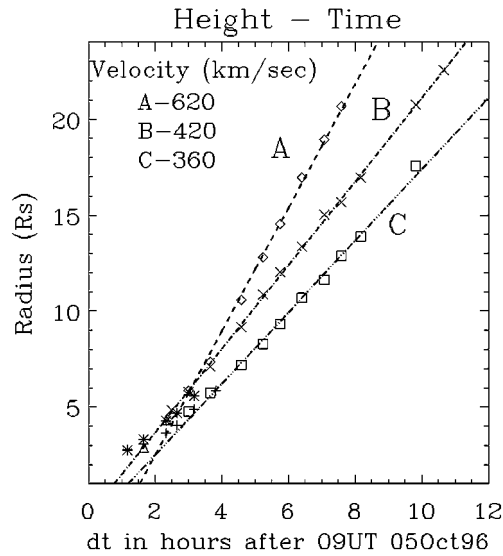


Figure 8. H-T plot of the five features identified in Figure 7(c). The C2 (C3) positions are indicated by the following symbols: A $\Delta$ ( $\diamond$ ), B\*(x), and C + ( $\square$ ). Also shown are the linear fits to the data and the speeds obtained from the fits using the C3 measurements only.

In the above paragraphs, we have briefly summarized the observations of two Type C CMEs. The two events are not typical. CME3 is one of the largest, brightest and fastest events recorded by LASCO. CME4 is unusually slow for a Type C event with speeds that are smaller than for CME1. These two examples do illustrate the key observational characteristics of Type C events. The H-T plots of the individual features are well fit by a constant speed. Both events have the appearance of bright arcs that move away from the Sun with little or no change in the structures. These events do not show the loop-like structures that are seen in the Type A events.

## 5. Discussion

This paper has presented observational evidence to support the view that there are two types of CMEs. The Type A events show acceleration in the C2 and C3 images, are usually seen to be associated with pre-existing helmet streamers, and are often associated with prominence eruptions and/or filament disappearance. The Type C events show constant speed in the C3 FOV. The Type C events often occur in close temporal association with X-ray flares.

Only limited analysis of LASCO CMEs has been published and the preliminary results are somewhat contradictory. St. Cyr *et al.* (1998) presented a preliminary analysis of LASCO observations for May-July, 1996. They measured the speed for 44 CMEs, and report that a linear fit 'appeared adequate' in 86% of those events. They also discuss the morphology of these event in terms of 'concave-outward'

structures (Burkepile and St. Cyr, 1983). For the 65 CMEs studied, they report 23 cases of the clear appearance of this feature and additional 13 case of the possible appearance. This morphology is considered to be a possible signature of magnetic disconnection and is usually associated with streamer-blowout CMEs (Webb and Cliver, 1995). The streamer-blowout CMEs usually show acceleration. The results reported by St Cyr *et al.* are not consistent with this picture.

A more complete analysis of the LASCO CMEs (1996 trough June 1998) was presented by St. Cyr *et al.* (2000). They measured the speed of 640 CMEs. The constant acceleration, second order fit, was ‘deemed appropriate’ for only 17% of these events. They report that the fraction of CMEs with significant acceleration was a function of the range of heights over which the measurements are made. CMEs measured over a greater range of heights were more likely to yield acceleration.

Tappin and Simnett (1997) report the measurement of height-time profiles for 149 CMEs occurring between May 1996 and August 1997. They report that 46% of these events showed constant acceleration, 22% showed step-wise acceleration, and only 27% showed a constant speed. They also report that many of the accelerated events seem to be launched from heights of about  $2.5 R_{\odot}$ . The constant speed events tend to be brighter, larger and faster than the other CMEs.

Sheeley *et al.* (1999) reported a new method of measuring height/time maps. They have measured a large number of CMEs using this technique, and conclude that there are two principal types of CMEs. When viewed on the limb, one class was accelerated while the other had uniform motions at higher speed. When viewed at positions away from the solar limb, one class exhibited gradual acceleration while the other had higher speeds with deceleration observed at large heights. These observations can be explained if the fast CMEs are decelerated, perhaps by the sweeping-up of coronal mass, at heights of approximately  $60-90 R_{\odot}$ . This study does not contain statistics or distribution of events. However, a large fraction of CMEs show acceleration (N. R. Sheeley, Jr., personal communication).

The above referenced studies are not consistent. Some of the difference is probably due to different analysis methods. However, a significant difference remains. Additional research is clearly required to determine what portion of the LASCO CMEs exhibit acceleration and to characterize the height range over which this acceleration is observed..

The four CMEs discussed in Sections 3 and 4 are all seen at positions close to the solar limb. This allows the structures to be clearly observed, and the observed morphology could be used to divide CMEs into classes. When CMEs are viewed at angles away from the plane-of- the-sky, it can become difficult to identify the morphological class of CMEs. The H-T plots can still be used to distinguish the two types: accelerated events will still produce curved H-T plots (Sheeley *et al.*, 1999).

There are other areas in which additional research is clearly needed. The Type A events have been associated with pre-existing helmet-streamers and prominence eruptions. The Type C events may be associated with X-ray flares and radio bursts.

These associations need to be tested by the systematic measurement and publication of H–T plots and movies for large numbers of CMEs. The studies needed to establish the relationships between CMEs, pre-existing coronal structures, and other forms of solar activity must be done.

We have presented two examples of CMEs showing a constant acceleration and two with constant speed. While the H–T plots are not the only way to identify the two types of events, this method does allow CMEs to be unambiguously placed into one of these two categories. While it would be most surprising if this simple two-type classification of CMEs were sufficient, it is our hope that this classification will provide a framework for the measurement and characterization of CMEs.

### Acknowledgements

The entire LASCO consortium has supported the ongoing research that made this paper possible. Discussions with M. Dryer, S. J. Plunkett, N. R. Sheeley, Jr., G. M. Simnett, S. J. Tappin, and S. T. Wu have been particularly helpful. NASA supports the LASCO Project at NRL under contract S-86760-E.

### References

- Andrews, M. D., Wang, A.-H., and Wu, S. T.: 1999, *Solar Phys.* **187**, 427–446.
- Andrews, M. D. and Howard, R. A.: 1999, *Solar Wind Nine*, in S. R. Habbal, R. Esser, J. V. Hollweg, and P. A. Isenberg (eds), AIP Conference Proceedings **471**, 629.
- Burkepile, J. T. and St. Cyr, O. C.: 1983, NCAR/TN-369+STR.
- Brueckner, G. E., *et al.*: 1995, *Solar Phys.* **162**, 357.
- Crooker, N., Joselyn, J. A. and Feynman, J. (eds): 1997, *Coronal Mass Ejections*, AGU Geophysical Monograph 90.
- Dryer, M.: 1996, *Solar Phys.* **169**, 421.
- Fleck, B., Domingo, V. and Poland, A. (eds): 1995, *The SOHO Mission*, Kluwer Academic Publishers, Dordrecht, Holland.
- Gosling, J. T.: 1997, in N. Crooker, J. A. Joselyn, and J. Feynman (eds), *Coronal Mass Ejections*, AGU Geophysical Monograph 90, 9.
- Gosling, J. T., Hildner, E., MacQueen, R. M., Munro, R. H., Poland, A. J. and Ross, C. L.: 1976, *Solar Phys.* **48**, 389.
- Howard, R. A., Brueckner, G. E., St. Cyr, O. C., *et al.*: in N. Crooker, J. A. Joselyn, and J. Feynman (eds), *Coronal Mass Ejections*, AGU Geophysical Monograph 90, 17.
- Howard, R. A., Sheeley, N. H., Koomen, M. J. and Michels, D. J.: 1985, *J. Geophys. Res.* **90**, 8173.
- Hundhausen, A. J.: 1993, *J. Geophys. Res.* **98**, 13,177.
- Hundhausen, A. J.: 1997, in N. Crooker, J. A. Joselyn, and J. Feynman (eds), *Coronal Mass Ejections*, AGU Geophysical Monograph 90, 1.
- Kahler, S.: 1987, *Rev. Geophys.* **25**, 663.
- Kahler, S.: 1988, *Proceeding of Solar Wind 6*, Boulder CO, NCAR, p. 215.
- Kahler, S.: 1992, *Ann. Rev. Astron. Astrophys.* **30**, 113.

- Koomen, M. J., Detwiler, C. R., Brueckner, G. E., Cooper, H. W. and Tousey, R.: 1975, *Appl. Optics* **14**, 743.
- Low, B. C.: 1996, *Solar Phys.* **167**, 217.
- Lyot, B.: 1930, *C.R. Acad. Sci. Paris* **191**, 834.
- MacQueen, R. M. and Fisher, R. R.: 1983, *Solar Phys.* **89**, 89.
- Munro, R. H., Gosling, J. T., Hildner, E., MacQueen, R. M., Poland, A. I. and Ross, C. L.: 1979, *Solar Phys.* **61**, 201.
- Maia, D., Vourlidis, A., Howard, R. A., Schwenn, R. and Magalhaes, A.: 1999, *J. Geophys. Res.* **102** (A6), 12,506.
- St.Cyr, O. C., Burkepile, J. T., Hundhausen, A. J. and Lecinski, A. H.: 1999, *J. Geophys. Res.* **104**, 12,493.
- St. Cyr, O. C., Howard, R. A., Simnett G. M., *et al.*: 1997, *Proc. 31st Eslab Symposium*, ESA SP-415, p. 103.
- St. Cyr, O. C., Howard, R. A., Sheeley, N. R., Jr., *et al.*: 2000, *J. Geophys. Res.*, in press.
- Sheeley, N. J., Jr., Watters, J. H., Wang, Y.-M., and Howard, R. A.: 1999, *J. Geophys. Res.* **104** (A11), 24,739.
- Strachan, L., *et al.*: 1999, *Solar Wind Nine*, in S. R. Habbal, R. Esser, J. V. Hollweg, and P. A. Isenberg (eds), AIP Conference Proceedings, Vol. 471, p. 637.
- Tousey, R.: 1973, *Adv. Space Res.* **13**, 713.
- Tappin, S. J. and Simnett, G. M.: 1997, *Proc. 31st Eslab Symposium*, ESA SP-415, 117.
- Wagner, W. J.: 1984, *Ann. Rev. Astron. Astrophys.* **22**, 267.
- Webb, D. F. and Cliver, E. W.: 1993, *J. Geophys. Res.* **100** (A4), 5853.
- Webb, D. F. and Hundhausen, A. J.: 1987, *Solar Phys.* **108**, 383.
- Wu, S. T., Guo, W. P., Andrews, M. D., *et al.*: 1997, *Solar Phys.* **175**, 719.
- Wu, S. T., Andrews, M. D. and Plunkett, S. P.: 2000, *Spac. Sci. Rev.* **95**, 147, this issue.